buildings

MDPI

Article

Simulation Analysis of the Small Wild Goose Pagoda Structure Using a Shape Memory Alloy-Suspension Pendulum Damping System (SMA-SPDS)

Tao Yang [1,*], Shuailei Liu [1], Shengyuan Xiong [1], Yang Liu [1], Bo Liu [2] and Binbin Li [3]

[1] School of Urban Planning and Municipal Engineering, Xi'an Polytechnic University, Xi'an 710600, China; liu13233724096@126.com (S.L.); wsdazxsy@126.com (S.X.); liuyang@xpu.edu.cn (Y.L.)
[2] Post-Doctoral Research Workstation, China Railway 20th Bureau Group Co., Ltd., Xi'an 710016, China; liubo208@xauat.edu.cn
[3] Key Laboratory of Structural Engineering and Earthquake Resistance, Ministry of Education (XAUAT), Xi'an 710055, China; libinbin@xauat.edu.cn
* Correspondence: yangtao@xpu.edu.cn

Abstract: To reduce the effects of earthquakes on the ancient Small Wild Goose Pagoda, a shape memory alloy-suspension pendulum damping system (SMA-SPDS) is developed by combining superelastic SMAs with damping pendulum theory. A MATLAB/Simulink simulation model of the SMA-SPDS is established and tested on a 1:10 scale model of the Pagoda. After verifying and comparing the simulation data with experimental results, a shock absorption analysis is performed on the prototype Pagoda. The optimum engineering design for the prototype structure of the Small Wild Goose Pagoda using SMA-SPDS for shock absorption protection in the future is put forward. The results show that the performance of the SMA-SPDS system is stable, and it can improve the integrity of the original structure of the Pagoda for better performance during earthquakes. In addition, with an increment in seismic intensity, the SMA-SPDS shows an apparent controlling effect. The Simulink simulation results of the model structure of the Small Wild Goose Pagoda are in good agreement with the test results. The Simulink simulation method can simulate the seismic response of the model structure of the Small Wild Goose Pagoda well, with and without SMA-SPDS, to obtain a more real damping effect of setting SMA-SPDS on the prototype structure; The engineering optimization of the location, quantity, and system performance parameters of SMA-SPDS in the prototype structure of the Small Wild Goose Pagoda has a remarkable effect, which can make the damping effect of SMA-SPDS reach more than 43% floor.

Keywords: small wild goose pagoda; SMA-SPDS; shaking table test; simulation analysis; seismic response; MATLAB

Citation: Yang, T.; Liu, S.; Xiong, S.; Liu, Y.; Liu, B.; Li, B. Simulation Analysis of the Small Wild Goose Pagoda Structure Using a Shape Memory Alloy-Suspension Pendulum Damping System (SMA-SPDS). *Buildings* **2022**, *12*, 686. https://doi.org/10.3390/buildings12050686

Academic Editors: Fernando F. S. Pinho and Humberto Varum

Received: 7 April 2022
Accepted: 17 May 2022
Published: 20 May 2022

1. Introduction

China is an ancient civilization with a long history. As a part of Chinese history and culture, ancient pagodas play an extremely important role in the history of Chinese architecture [1]. As an outstanding representative of an ancient pagoda that shows the early use of dense eaves in China, the Small Wild Goose Pagoda has attracted much attention at home and abroad because of its unique historical value and cultural connotation. However, as the Pagoda has stood for thousands of years, it has experienced the vicissitudes of history and man-made destruction, the tower body has been damaged to varying degrees, its seismic performance has been severely reduced, and it will be difficult for the Pagoda to withstand more earthquakes in the future. Therefore, the protection and ability of the Small Wild Goose Pagoda to resist disasters is an important issue [2]. Figure 1 shows the extant Small Wild Goose Pagoda.

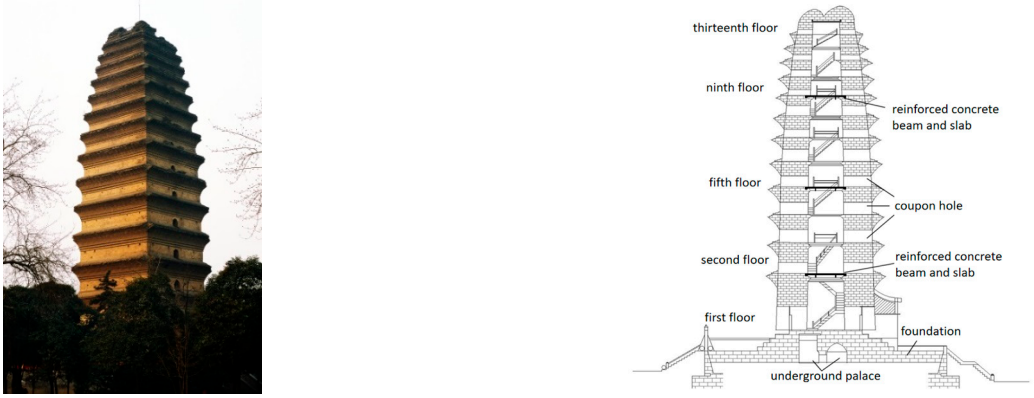

(**a**) (**b**)

Figure 1. The extant Small Wild Goose Pagoda. (**a**) Live-action. (**b**) Section drawing.

In recent years, scholars worldwide have conducted extensive research on the seismic protection of masonry ancient towers [3–5]. According to their seismic response characteristics of ancient towers, they put forward suggestions to strengthen their seismic capacity, including tower hooping [6], crack bonding [7], adding a circle beam and constructional column [8], the use of high ductility fiber-reinforced cement-based composite reinforcement [9], and the installation of foundation isolation [10]. However, the traditional seismic protection methods are not in agreement with the minimum intervention principle of ancient building protection because of their excessive disturbance of the structure itself. Therefore, structural vibration control has been proposed as a new theory and method to effectively reduce the seismic response of structures, and its use has been verified.

As a part of structural vibration control, passive control is widely used in all kinds of building structural systems [11,12] because this approach does not need an external energy input, uses simple devices, and has a significant effect on energy consumption. However, there are still many shortcomings in the passive control devices that have been developed and applied. For example, viscoelastic dampers have a short service life, friction dampers have unstable friction coefficients, and mild steel dampers undergo irreversible plastic deformation. Although viscous dampers can provide a very large damping force for a structure, their effects are velocity-dependent, they have poor energy dissipation under low-frequency and ultrahigh-frequency loads, and they lack the ability to reset. After an earthquake, the structure experiences residual strain [13,14].

With the popularization of new materials, especially shape memory alloys (SMAs), a new path has been opened for the field of structural vibration control. Shape memory alloys have a unique shape memory effect, hyperelasticity, and high damping properties. SMA dampers developed in the field of civil engineering have the advantages of good durability, corrosion resistance, long service cycles, the capacity for large deformations, and the ability to reset [15–17]. Dieng et al. [18] designed an SMA damper with 2.5 mm diameter nickel-titanium alloy wire and carried out a control test on a 50 m long stay cable. The results show that the damper can reduce the displacement amplitude by 75%. Asgarian et al. [19] proposed a new type of self-resetting hybrid damper. The results of the nonlinear analysis of time records for a five-story controlled structure showed that the damper could effectively control the roof acceleration, inter-story displacement, and plastic deformation of the structure. Kari et al. [20] developed a double support system composed of an SMA support and buckling restraint support, which could effectively reduce the inter-floor displacement and residual deformation of steel structures.

This paper discusses a study of the advantages of a combination of structural vibration control technology and shape memory alloys. A shape memory alloy-suspension pendulum damping system (SMA-SPDS) was designed and made in this laboratory. The goal of this study was to study the energy dissipation and damping effect of the SMA-SPDS for possible use in the Small Wild Goose Pagoda. Considering the size of the shaking table, the study

takes the size similarity coefficient of 1/10 to make a scale prototype of the Pagoda [21]. A shaking table test of the model Pagoda was performed, and Simulink was used to simulate its response with the SMA-SPDS under the action of seismic waves. The test results were compared with the simulation analysis to verify the correctness of the simulation model and calculation method. Finally, the simulation model was applied to the prototype structure of the Pagoda to optimize and analyze its damping effect. The results showed that the SMA-SPDS can be used for seismic protection of the Small Wild Goose Pagoda, and it showed promise for engineering applications to similar ancient masonry pagoda structures.

2. Shape Memory Alloy and Suspension Pendulum Damping System

2.1. SMA-SPDS Structural Design

Combining the phase-change pseudoelasticity of the SMA wire and the pendulum theory, an SMA-SPDS was designed (see Figure 2). The whole system consisted of a mass vibrator, a pendulum rod, a one-way hinge, a slider, an SMA wire (the diameter is 1.0 mm, and the phase transition temperature was as follows: M_f was −42 °C, M_s was −38 °C, A_f was −13 °C, and A_s was −9 °C), a baffle plate, and a diverting pulley. Its structural design was as follows: (1) As the connection point of the upper end of the swing rod, the one-way hinge is perpendicular to the swing plane. The upper end of the swing rod is provided with a penetration hole, which could freely penetrate into the one-way hinge rotating shaft. Threads are set at both ends of the rotating shaft, and the middle is smooth enough to ensure the free rotation of the swing rod. (2) The lower end of the swing rod is connected with the screw hole at the center of the mass vibrator, and a plurality of installation points are symmetrically arranged on the mass vibrator to facilitate the adjustment of the mass. (3) One end of the SMA wire on both sides of the mass vibrator passes through the slider baffle and is connected with the slider. After passing through the steering pulley, the other end is fixed to the structure after being connected with the steel cable through the conversion joint.

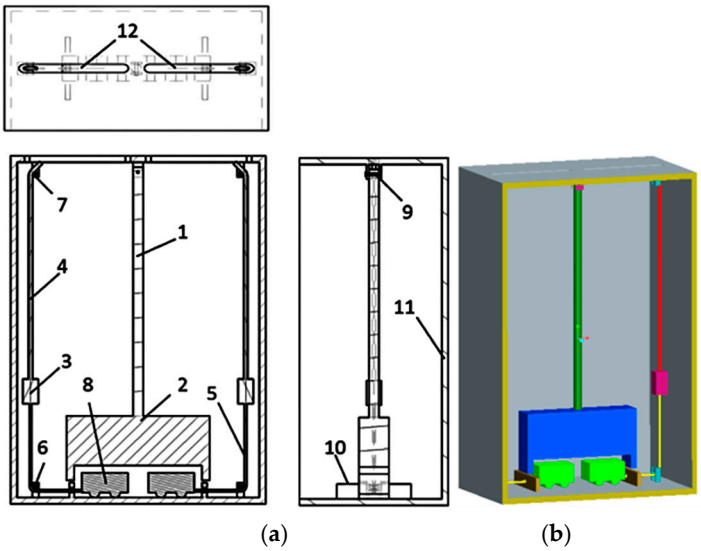

Figure 2. SMA-SPDS structure diagram. (**a**) Construction details. (**b**) Three-dimensional structure. 1—Pendulum rod; 2—Mass vibrator; 3—Wire conversion joint; 4—Steel cable; 5—SMA; 6—Bottom steering pulley; 7—Upper steering pulley; 8—The small car; 9—One-way hinge; 10—Baffle; 11—The shell; 12—Steel cable channel.

2.2. SMA-SPDS Working Mechanism

Taking one cycle as an example to illustrate the working principle and process of the proposed SMA-SPDS, when the earthquake effect is small, the mass vibrator can swing freely without contacting the slider, and the reverse inertial force acts through the rigid outer wall above the structure. When the tower body is greatly affected by an earthquake,

the mass vibrator moves with the slider. If the structure vibrates to the right, then the mass vibrator swings to the left and drives the right slider with the horizontal slide, pulling the right side of the SMA wire so that it is relatively displaced while the SMA wire on the left side is still at rest. When the mass vibrator returns to the equilibrium position, the SMA wire returns to the initial pretension state, the right SMA wire undergoes an energy-consuming cycle with a full hysteresis curve, and the energy dissipation of the structure is realized. Additionally, the inertial force of the mass vibrator reacts to the structure through the steel cable, which suppresses the seismic response of the structure, thereby attenuating the seismic response of the structure. The principle of the mass vibrator moving to the right is the same.

The pendulum damping system is a type of damping system that can be set in an ancient tower structure. However, if the pendulum damping system is set only on the internal floor of an ancient tower structure, it has a small damping effect because of its characteristics. If the suspension damping system is combined with an SMA wire and an SMA-SPDS with a good performance that was developed by connecting the wire steel cable with the ancient tower structure, the inertial force of the suspension damping system can be transmitted to the ancient tower structure through the wire steel cable. Additionally, the SMA wire in the SMA-SPDS can provide damping to dissipate energy and absorb shock, significantly reducing the seismic response of the ancient tower structure.

3. Shaking Table Test Analysis of the Small Wild Goose Pagoda Structure with SMA-SPDS

3.1. Small Wild Goose Pagoda Test Model

This model was designed and fabricated based on the present condition of the Pagoda after it was repaired in 1965. In addition, the model accounts for the size and carrying capacity of the shaking table. The similarity coefficient of the size is 1/10, and the total height is 4 m. The model design adopts the method of short artificial mass. The weight is set in the weight box of the tower wall. The masonry material used in the model of the Small Wild Goose Pagoda structure is blue brick after the cutting process. There are two main bricks with specifications as follows: the main body structure brick is 110 mm × 50 mm × 25 mm, and the eaves brick is 110 mm × 50 mm × 10 mm. The tower sizes and overall models are shown in Figure 3. The coupon cave is the weakest part of the structure of the Pagoda. Therefore, in this test, one SMA-SPDS along the weak stiffness direction of the coupon hole is set at the first, second, and fifth floors of the model structure of the Pagoda, and the top connection method is adopted. The arrangement and connection of the SMA-SPDS in the Small Wild Goose Pagoda are shown in Figure 4. The SMA wire is connected with a steel cable through the wire cable adapter, passes through the steering pulleys at the bottom and top of the SMA-SPDS, and then is fixed at the bottom plate of the structure.

(**a**) (**b**)

Figure 3. Tower dimensions and overall model. (**a**) Tower size; (**b**) Overall model.

(**a**) (**b**)

Figure 4. SMA-SPDS installation setup diagram. (**a**) SMA-SPDS connection; (**b**) SMA-SPDS installation.

As the selected material of the model is brick masonry, its bearing capacity and other parameters are basically the same as those of the prototype structure, which is desirable. According to Buckingham theory and dimensional analysis, the similarity relationship between the model and prototype structure is calculated to obtain the similarity coefficients of this test, as shown in Table 1.

Table 1. Model similarity relation table.

Similar Physical Quantity	Symbol	Formula	Similarity Ratio
size	S_l	model l/archetype l	0.1
elasticity modulus	S_E	model E/archetype E	1
mass	S_m	Model m/archetype m	0.00361
density	S_ρ	$S_\rho = S_m/{S_l}^3$	3.61
accelerated velocity	S_a	$S_a = S_E\ {S_l}^2/S_m$	2.77
stress	S_σ	$S_\sigma = S_E/S_a$	0.361
time	S_t	$S_t = \sqrt{S_l/S_a}$	0.19
displacement	S_w	$S_w = S_l$	0.1
velocity	S_v	$S_v = \sqrt{S_l S_a}$	0.526
frequency	S_f	$S_f = 1/S_t$	5.26

3.2. Experimental Plan

The experiment was conducted in the Seismic Laboratory of Structural Engineering of Xi'an University of Architecture and Technology. The test adopted a 3-way 6-degree-of-freedom electrohydraulic servo simulation control vibrator produced by MTS, USA. The parameters were as follows: the size of the vibration table was 4.1 m × 4.1 m; the weight of the fully-loaded specimen was 30T; the maximum horizontal acceleration at full load was 1.5 g; the maximum vertical acceleration was 1.0 g; the maximum overturning bending moment was 80 T.m; the maximum eccentric bending moment was 30 T.m (Figure 5a). A PCB acceleration sensor and a type 891 displacement sensor were used for the acceleration and displacement data, and an LMS data acquisition instrument was used for the test data collection (Figure 5b).

According to the "Code for Seismic Design of Buildings" [22] records for two strong actual earthquakes, the El Centro record (north–south direction), the Jiangyou seismic record (east–west direction), and one artificial wave, the Shanghai wave, were selected for the simulated seismic shaking table test. According to the test scheme, the simulated shaking table test of the model structure of the Small Wild Goose Pagoda under nine working conditions of an 8-degree small earthquake (0.2 g), 8-degree medium earthquake (0.6 g), and 8-degree large earthquake (0.9 g) was carried out under three kinds of seismic waves. The experimental results were recorded and compared with the results for the Small Wild Goose Pagoda model, with and without the proposed SMA-SPDS.

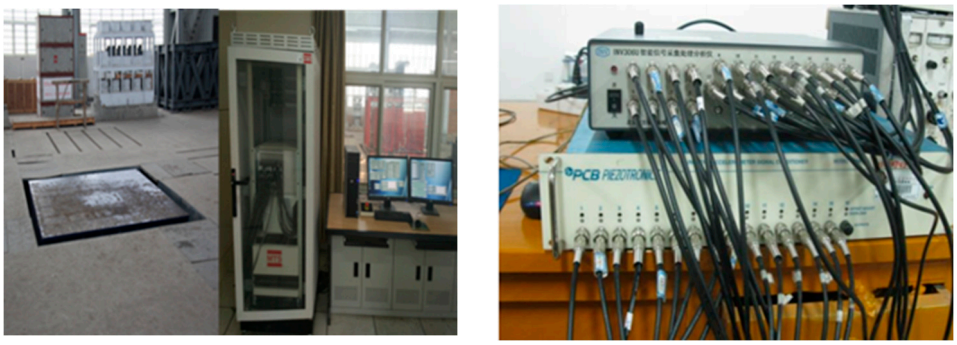

(**a**) (**b**)

Figure 5. Testing equipment. (**a**) Field of shaking table and control system; (**b**) LMS data acquisition instrument (under test).

3.3. Analysis of Model Shaking Table Test Results

3.3.1. Model Structure Dynamic Characteristics

The white noise sweeping technique for the shake table test is widely used to test the dynamic characteristics of structures after earthquakes of different intensities. Therefore, after performing the same intensity earthquake in the test, white noise with a peak acceleration of 50 gal was employed as a sweep input to test the structural acceleration response of the model and obtain the natural vibration (self-vibration) frequency of the Small Wild Goose Pagoda model structure. The natural vibration frequency and period of the Small Wild Goose Pagoda model structure are listed (see Table 2).

Table 2. Natural vibration frequency and period of the Small Wild Goose Pagoda model structure.

Test Condition		Lowest Frequency		Second Frequency	
		Frequency (Hz)	Period (s)	Frequency (Hz)	Period (s)
Without control	Before the earthquake	5.83	0.17	14.13	0.071
	Small earthquake	5.31	0.19	14.12	0.071
	Medium earthquake	5.05	0.20	13.98	0.072
	Large earthquake	4.71	0.21	13.81	0.072
With control	Before the earthquake	6.08	0.16	15.23	0.066
	Small earthquake	5.98	0.17	15.23	0.066
	Medium earthquake	5.93	0.17	14.97	0.067
	Large earthquake	5.45	0.18	14.97	0.067

3.3.2. Analysis of the Acceleration Response of the Model Structure

Under the action of different seismic waves, the acceleration response of the Small Wild Goose Pagoda model was basically consistent with the spectrogram of the input seismic waves, and the response interval was concentrated at the peak of the acceleration input. As the magnitude of the seismic wave decreased, the structural response decreased as well. Under the action of different seismic waves, the model structure had multiple points with large acceleration response values, especially for the performance of the Jiangyou seismic record. The peak responses of the acceleration of the Small Wild Goose Pagoda are listed (see Tables 3 and 4 and Figure 6; the direction is X direction).

Table 3. The extremum acceleration of the top floor of the tower with no control condition under 8-degree earthquakes (g).

	El−Centro Wave		Jiangyou Wave		Artificial Wave	
	Max	Min	Max	Min	Max	Min
Small earthquake	0.647	−0.661	0.603	−0.624	0.688	−0.694
Medium earthquake	1.231	−1.304	1.770	−1.815	1.972	−1.938
Large earthquake	1.813	−1.914	2.354	−2.460	2.664	−2.589

Table 4. The extremum acceleration of the top floor of the tower with control condition under 8-degree earthquakes (g).

	El−Centro Wave		Jiangyou Wave		Artificial Wave	
	Max	**Min**	**Max**	**Min**	**Max**	**Min**
Small earthquake	0.552	−0.570	0.512	−0.528	0.587	−0.604
Medium earthquake	0.886	−0.937	1.338	−1.387	1.461	−1.474
Large earthquake	1.239	−1.458	1.739	−1.782	1.830	−1.714

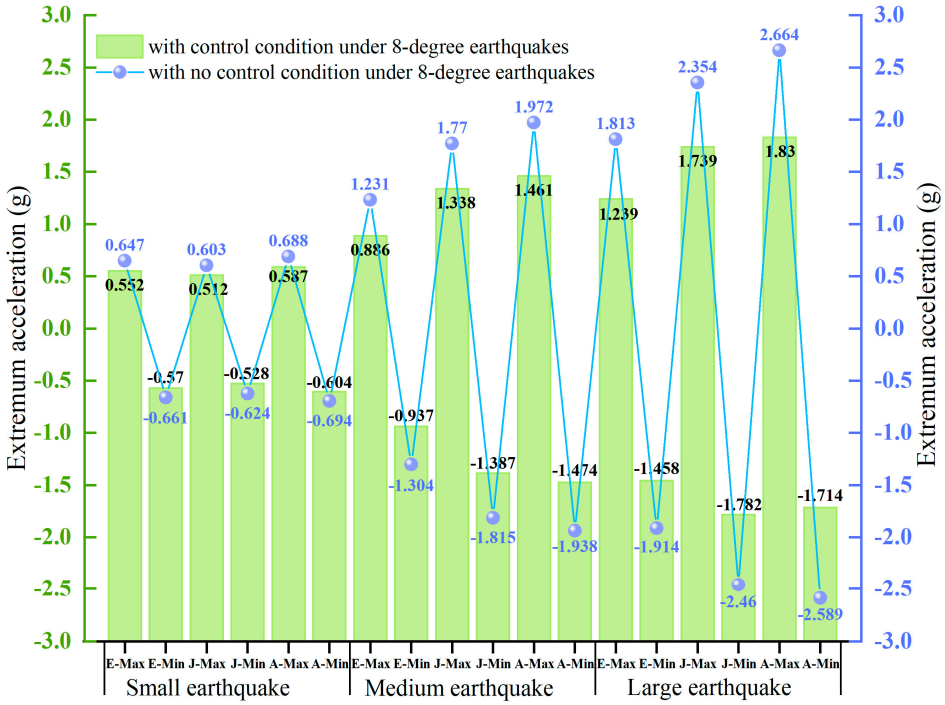

Figure 6. The peak responses of the acceleration of the Small Wild Goose Pagoda. (Note: in the x-coordinate, the letter E stands for "El-Centro Wave"; the letter J refers to Jiangyou Wave; the letter A stands for Artificial Wave.)

3.3.3. Analysis of the Displacement Response of the Model Structure

The relative displacements of multiple floors of the Small Wild Goose Pagoda are shown (see Tables 5 and 6, Figure 7).

Table 5. The maximum relative displacement of the top floor of the tower with no control condition under 8-degree earthquakes (mm).

	El-Centro Wave		Jiangyou Wave		Artificial Wave	
	Measured Displacement	**Relative Displacement**	**Measured Displacement**	**Relative Displacement**	**Measured Displacement**	**Relative Displacement**
Small earthquake	5.011	3.197	4.354	2.094	15.16	5.318
Medium earthquake	9.485	5.819	8.169	3.530	28.89	10.19
Large earthquake	16.84	11.87	12.23	5.908	62.06	31.83

Table 6. The maximum relative displacement of the top floor of the tower with control condition under 8-degree earthquakes (mm).

	El-Centro Wave		Jiangyou Wave		Artificial Wave	
	Measured Displacement	Relative Displacement	Measured Displacement	Relative Displacement	Measured Displacement	Relative Displacement
Small earthquake	3.550	2.021	3.594	1.376	13.87	3.509
Medium earthquake	7.668	4.117	7.068	2.442	23.97	7.057
Large earthquake	13.21	8.051	10.03	4.098	49.49	23.32

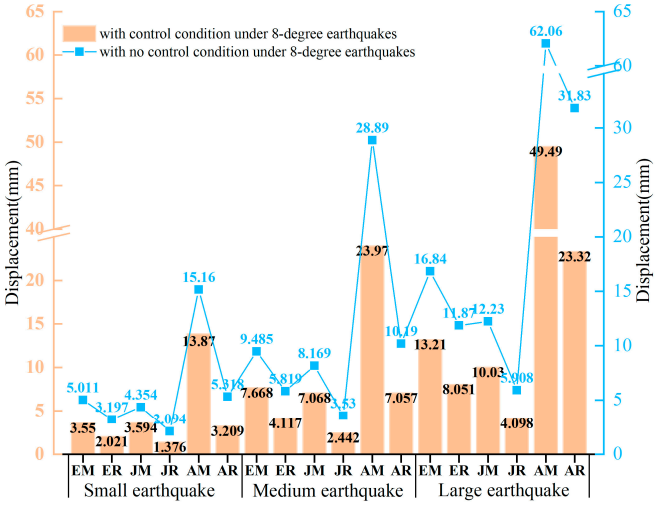

Figure 7. The relative displacements of multiple floors of the Small Wild Goose Pagoda. (Note: in the x-coordinate, the letter E stands for "El-Centro Wave"; the letter J refers to Jiangyou Wave; the letter A stands for "Artificial Wave"; the letter M stands for "Measured displacement"; the letter R stands for "Relative Displacement".)

4. Simulation Process of the Small Wild Goose Pagoda Structure with a Damping System

The Small Wild Goose Pagoda structure was assumed to be infinitely rigid in the plane of the slab, and torsional effects were not considered. The inter-floor shear series multiple-degree-of-freedom vibration model was used for the analysis. The Small Wild Goose Pagoda structure with the SMA-SPDS was divided into two parts: the main structure of the Pagoda and the SMA-SPDS. The equations of motion are listed separately.

4.1. Establishment of the Simulation Model of the Small Wild Goose Pagoda Structure

Considering the role of the SMA-SPDS, the motion equation of the main structure of the Small Wild Goose Pagoda can be expressed as:

$$M\ddot{x} + C\dot{x} + Kx = -M\ddot{x}_g + P^T f \quad (1)$$

where P is for the $n \times m$-order setting matrix; m is the number of damping devices, whose value is one at the damping system setting position, with the remaining elements 0; M, C, and K are the mass matrix, damping matrix, and stiffness matrix of the small goose tower structure, respectively; f represents the passive control force vector; and $f = \bar{C}(\dot{\bar{x}} - P\dot{x}) + \bar{K}(\bar{x} - P\bar{x})$, $\bar{M}$, $\bar{C}$, and $\bar{K}$ are the mass matrix, damping matrix, and stiffness matrix of SMA-SPDS, respectively, where x and $\dot{\bar{x}}$ are the displacement vector and velocity vector of the damping device, respectively.

We introduce a state vector $Z = \begin{bmatrix} x(t) \\ \dot{x}(t) \end{bmatrix}_{2n\times 1}$; then, the space equation of the main structure of the Small Wild Goose Pagoda is:

$$\begin{cases} \dot{Z}(t) = AZ(t) + BU(t) \\ Y(t) = CZ(t) + DU(t) \end{cases} \tag{2}$$

where $Y(t)$ is the output matrix for the system, $U(t) = -M\{1\}\ddot{x}_g + P^T f; C = [I]_{2n\times 2n}$; $D = [0]_{2n\times n}$; $A = \begin{bmatrix} 0_{n\times n} & I_{n\times n} \\ -M^{-1}K & -M^{-1}C \end{bmatrix}_{2n\times 2n}$; $B = \begin{Bmatrix} 0_{n\times n} \\ M^{-1} \end{Bmatrix}_{2n\times n}$; $[I]$ and $[0]$ are the unit matrix and zero matrix, respectively, whose dimensions are $2 \times 2\ n$ or $n \times n$.

From this state equation, the displacement and velocity of the main structure of the Small Wild Goose Pagoda relative to the ground can be solved, while the acceleration is not suitable for the derivative derivation module in Simulink. The output of the derivative module can be solved by an approximate value. To reduce the error of the result, the structural acceleration can be directly obtained by the following formula:

$$\ddot{x} = M^{-1}\left(-M\ddot{x}_g + P^T f - C\dot{x} - Kx\right) \tag{3}$$

Figures 8 and 9 show the main structure of the Small Wild Goose Pagoda and the passive control force Simulink simulation model.

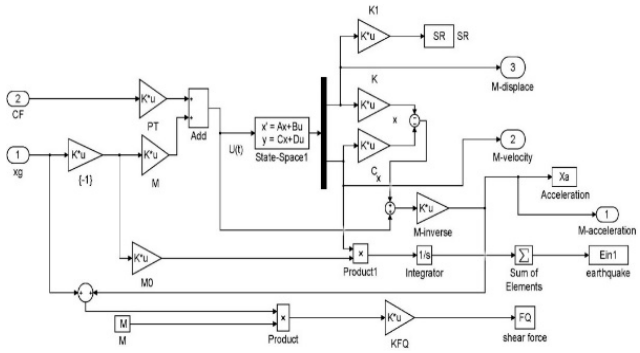

Figure 8. Simulation model of the main structure of the Small Wild Goose Pagoda.

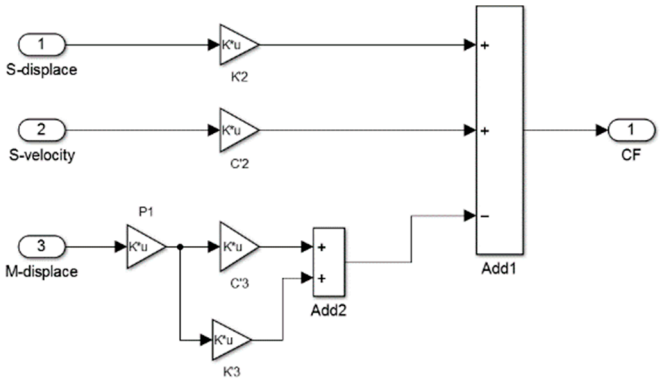

Figure 9. Passive control force simulation model.

4.2. Establishment of the SMA-SPDS Simulation Model

The equation of motion for the SMA-SPDS is

$$\bar{M}P\ddot{x} + \bar{M}\left(\bar{\ddot{x}} - P\ddot{x}\right) + \bar{C}\left(\bar{\dot{x}} - P\dot{x}\right) + K\left(\bar{x} - P\bar{x}\right) = -\bar{M}I\ddot{x}_g \tag{4}$$

Referring to the establishment of the simulation model of the Small Wild Goose Pagoda in Section 4.1, the acceleration vector expression of the SMA-SPDS damping device can be obtained (5):

$$\ddot{\bar{x}} = \bar{M}\left(-\bar{M}\ddot{x}_g + \bar{C}P^T\dot{x} + \bar{K}P^T x - \bar{C}\dot{\bar{x}} - \bar{K}\bar{x}\right) \quad (5)$$

The Simulink simulation model of the SMA-SPDS is given in Figure 10.

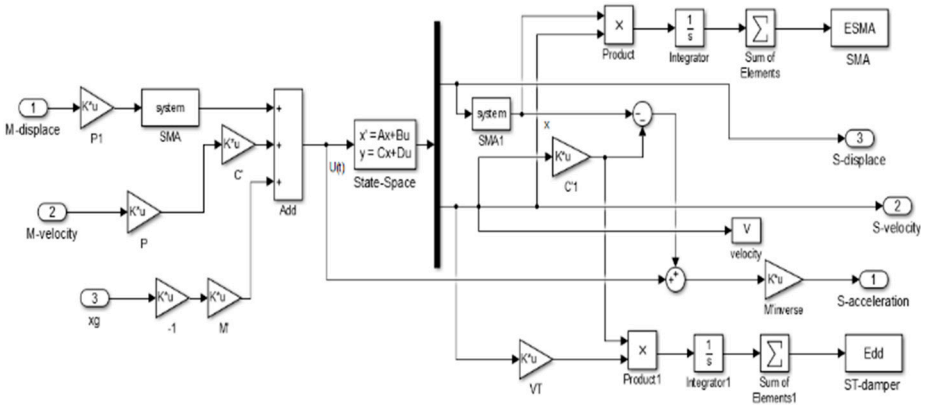

Figure 10. SMA-SPDS simulation model.

4.3. Energy Response Simulation Model

When the structure of the prototype Small Wild Goose Pagoda with the SMA-SPDS undergoes earthquakes, most of the seismic energy is dissipated by the damping system. Therefore, the energy dissipation capacity of the damping system directly affects the seismic resistance and performance of the Pagoda structure.

By integrating and organizing the absolute displacement of the motion equation (Formula (4)) of the small goose tower structure with SMA-SPDS, the energy balance equation can be simplified as Formula (6):

$$E(t) = E_k(t) + E_c(t) + E_e(t) + E_d(t) \quad (6)$$

The items in the above formula are defined as follows: $E(t) = -\int_0^t \dot{x}^T M\{I\}\ddot{x}_g dt$; $E_k(t) = \int_0^t \dot{x}^T M\ddot{x} dt$; $E_c(t) = \int_0^t \dot{x}^T C\dot{x} dt$; $E_e(t) = \int_0^t \dot{x}^T Kx dt$; $E_d = \int_0^t \dot{x}^T F(x) dt = E_{SMA}(t) + E_{dd}(t)$. $E(t)$ is the total energy input into the structure by the earthquake at time t; $E_k(t)$ is the kinetic energy of the small goose tower structural system at time t;

$E_e(t)$ is the deformation energy of the structural system at time t; $E_c(t)$ is the damping energy dissipation of the structural system at time t; $E_d(t)$ is the energy consumption of the shock absorption system at time t; E_{SMA} is the energy consumption of SMA wire in the shock absorption system at time t. $E_{dd}(t)$ is the damping energy dissipation of the damping system at time t.

This equation is a simulation model of the main structural energy response of the prototype Small Wild Goose Pagoda, as shown in Figure 11.

4.4. Simulink Simulation Model

The main simulation model of the Small Wild Goose Pagoda shock absorption structure in Simulink is shown in Figure 12. The model consists of four major subsystems: the main structure, SMA-SPDS, control force, and main structure energy. The two inputs x_g and CF are the seismic acceleration and passive control force, respectively. The three outputs M-acceleration, M-velocity, and M-displacement are the acceleration, velocity, and displacement of the main structure of the Small Wild Goose Pagoda relative to the ground, respectively. E_k, E_e, and E_c are the kinetic energy, deformation energy, and damping energy consumption of the main structure of the Small Wild Goose Pagoda, respectively.

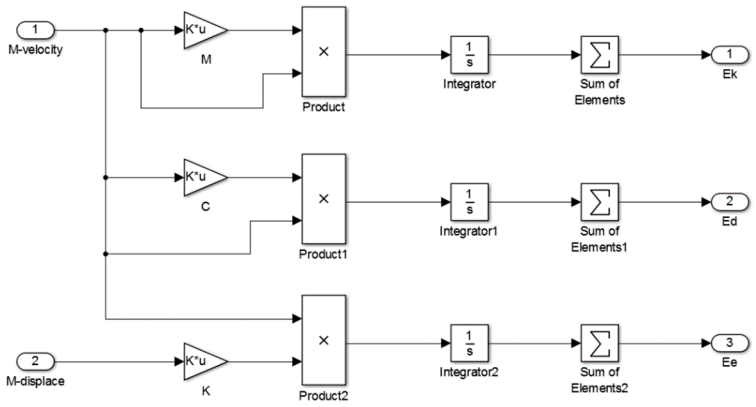

Figure 11. Simulation model of the main structure energy response of the Small Wild Goose Pagoda.

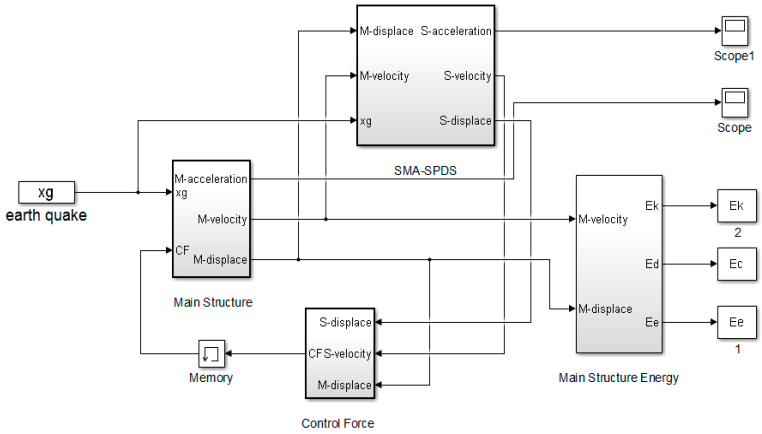

Figure 12. Main model of the Small Wild Goose Pagoda shock absorption structure.

4.5. Comparison of the Simulation and Test Results

The above test results were compared with simulation results calculated by Simulink to validate the feasibility of Simulink. The Simulink simulation and test results of the prototype Small Wild Goose Pagoda, with and without the SMA-SPDS, are shown in Figures 13 and 14.

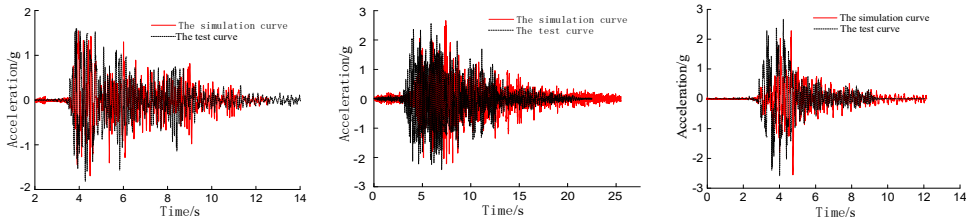

Figure 13. Comparison diagram of the acceleration simulation and test on top of an uncontrolled tower under an 8-degree large earthquake. (**a**) El-Centro record. (**b**) Jiangyou record. (**c**) Artificial wave.

Under the action of different seismic waves, the acceleration response of the Small Wild Goose Pagoda model was basically consistent with the spectrogram of the input seismic waves; the response interval was concentrated at the peak of the acceleration input. As the magnitude of the seismic wave decreased, the structural response decreased as well. Under the action of different seismic waves, the model structure had multiple points with large acceleration response values, especially for the seismic record.

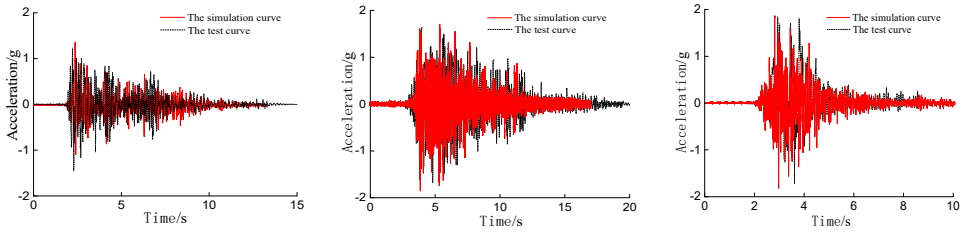

(**a**) (**b**) (**c**)

Figure 14. Comparison diagram of the acceleration simulation and test on top of a controlled tower under an 8-degree large earthquake. (**a**) El-Centro record. (**b**) Jiangyou record. (**c**) Artificial wave.

In the different test processes, the acceleration response of the structure of the Small Wild Goose Pagoda increased with increasing earthquake amplitude, and the response of the top of the tower increased from the initial value of 0.6 g to 2.58 g. After setting the SMA-SPDS in the model structure, the acceleration response caused by the earthquake was significantly smaller; the average decrease was approximately 15%. The results indicated that the proposed system had a good capability for damping in the Small Wild Goose Pagoda structure.

Figures 13 and 14 show that the Simulink simulation results for the Small Wild Goose Pagoda model structure were in good agreement with the experimental results. The Simulink simulation method can be used to simulate the seismic response of the Small Wild Goose Pagoda model and the SMA-SPDS. The above Simulink simulation program can be applied to simulate the seismic response of the original structure of the Small Wild Goose Pagoda to obtain a more realistic damping effect.

5. Simulation Analysis and Optimization of the Small Wild Goose Pagoda Tower Structure

5.1. SMA-SPDS Location Optimization

The SMA-SPDS developed in this paper achieved its vibration reduction effect by controlling the vibration mode of the Small Wild Goose Pagoda structure. Therefore, the SMA-SPDS should be tuned according to the vibration modes of the structure. Through the thoughtful selection of the location of the system configuration, the multiple-degree-of-freedom system can control the vibration of each modality, and vibrational damping should be configured at the most effective place without interfering with other modal operations. According to the equivalent quality concept [23,24], (1) the equivalent mass is the smallest in the vibration antinode (maximum amplitude point) of a certain model, and (2) the equivalent mass is infinite at a vibration node of a certain mode (amplitude is 0).

The dynamic characteristics of the Small Wild Goose Pagoda in the horizontal direction, such as its vibration frequency, damping ratio, and vibration mode, were obtained by on-site testing of the original structure. The vibration frequency and damping ratio are shown in Table 7, and the mode shape is shown in Figure 15.

Table 7. The Small Wild Goose Pagoda dynamic characteristic value.

Project	Level 1	Level 2	Level 3
Frequency (Hz)	1.348	3.401	5.303
Cycle (s)	0.74	0.29	0.19
Damping ratio/%	0.902	2.201	6.560

The on-site dynamic test was performed to determine the position of the SMA-SPDS arrangement for the Small Wild Goose Pagoda: the first location was set at the top floor to control the first-order mode; another location was set at the ninth floor to control the second-order mode; and the third-order mode should have also been set at the top floor.

Since the top floor was used as the first-order modal control point, the fifth floor was selected as the location for the SMA-SPDS control for the third-order mode.

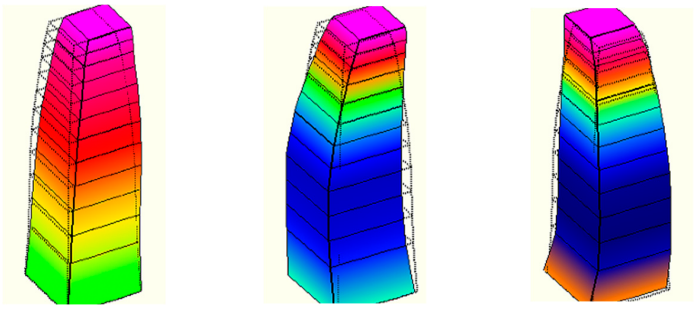

(**a**) (**b**) (**c**)

Figure 15. Mode modal diagram of the Small Wild Goose Pagoda. (**a**) First-level mode. (**b**) Second-level mode. (**c**) Third-level mode. (Note: the color change of each mode only indicates the amplitude change of that mode).

5.2. SMA-SPDS Parameter Optimization

Assuming that the structure has n SMA-SPDSs, an n degrees-of-freedom system can be established in the modal coordinates. Then, the structural motion equation with SMA-SPDS is:

$$[\phi]^T[G][\phi]\{\delta\} = [\phi]^T(\{F\} - \{F_d\}) \tag{7}$$

where F_d is the force vector for the SMA-SPDS; $[\phi] = [\{X_1\}\{X_2\}\cdots\{X_n\}] = \begin{bmatrix} \phi_{11} & \phi_{12} & \cdots & \phi_{1n} \\ \phi_{21} & \phi_{22} & \cdots & \phi_{2n} \\ \vdots & \vdots & \cdots & \vdots \\ \phi_{n1} & \phi_{n2} & \cdots & \phi_{nn} \end{bmatrix}$, is the modal matrix; j stands for the coordinate number; ϕ_{ji} represents the ordinal number of coordinates; i represents the order of modes; and $\{\delta\}$ is the generalized coordinate vector. For $[G] = -\omega^2[M] + j\omega[C] + [K]$, where $[M]$ is modal mass; $[K]$ is modal stiffness; $[C]$ is the structural damping matrix. The force vector obtained by the SMA-SPDS is a function of the displacement vector $\{X\}$. Assuming that the transfer matrix is $[H]$, the force vector can be expressed as:

$$\{F_d\} = [H]\{X\} \tag{8}$$

Since multiple degree-of-freedom systems with the SMA-SPDSs can be decoupled into multiple single-degree-of-freedom systems, the mechanical model of a single-degree-of-freedom system with the SMA-SPDSs in the i-order mode can be obtained as shown in Figure 16. The mass, SMA stiffness, and damping coefficient of the system are m_{di}, k_{di}, and c_{di}, respectively.

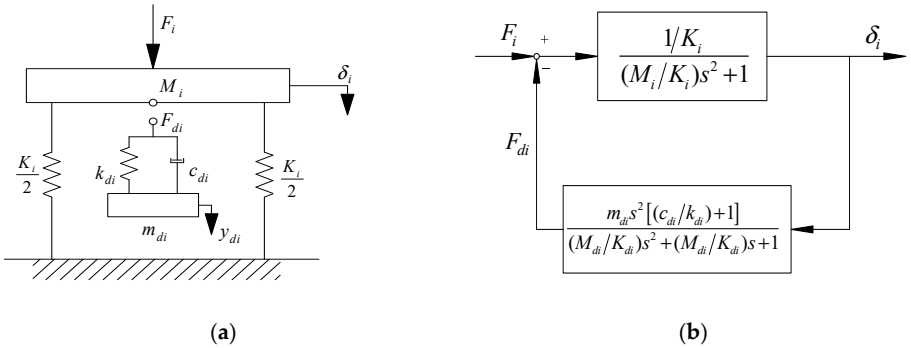

(**a**) (**b**)

Figure 16. A simplified model diagram of the vibration reduction system is added to the single-degree-of-freedom system of the i-th Mode. (**a**) Mechanical model. (**b**) Control flow chart.

The force generated by attaching the SMA-SPDSs F_{di} is represented by the following formula:

$$F_{di} = \frac{-m_{di}\omega^2(k_{di} - jc_{di}\omega)}{k_{di} - m_{di}\omega^2 + jc_{di}\omega}\delta_i \tag{9}$$

The SMA-SPDS provides feedback compensation. The transfer function G_{di} is derived as:

$$\frac{\delta_i}{F_i} = G_{di} \tag{10}$$

where G_{di} is the transfer function that contains the i-order mode in the damping system.

$$G_{di} = \frac{1 - (\frac{\omega}{\omega_{di}})^2 + 2j\zeta_i\left(\frac{\omega}{\omega_{di}}\right)}{(\frac{\omega}{\Omega_i})^2(\frac{\omega}{\omega_{di}})^2 - \left\{(\frac{\omega}{\omega_{di}})^2 + (\frac{\omega}{\Omega_i})^2(1+\mu_i)\right\} + 2j\zeta_i\left(\frac{\omega}{\omega_{di}}\right)\left(\frac{\omega}{\omega_{di}}\right)\left\{1 - (\frac{\omega}{\Omega_i})^2(1+\mu_i)\right\}}\frac{1}{K_i} \tag{11}$$

where $\omega_{di} = \sqrt{\frac{k_{di}}{m_{di}}}$, $\zeta_i = \frac{c_{di}}{2m_{di}\omega_i}$, and $\mu_i = \frac{m_{di}}{M_i}$. ω_{di}, ζ_i, and μ_i are the natural frequency, damping ratio, and mass ratio of the i-order mode in the damping system, respectively.

In this paper, the optimal design of the SMA-SPDS was based on fixed-point theory; the core idea was to find a specific point unrelated to the damping on the frequency response curve of the damped vibration system and use the specific point to perform the vibrational damping.

Assuming a single-degree-of-freedom damping system with a damping parameter, ζ, the frequency transfer function is expressed as:

$$G(\omega) = \frac{C(\omega) + \zeta D(\omega)}{A(\omega) + \zeta B(\omega)} \tag{12}$$

where $C(\omega)$ and $A(\omega)$ are the coefficient terms without ζ, and $D(\omega)$ and $B(\omega)$ are the coefficient terms with ζ. When $\zeta = 0$, the frequency transfer function is:

$$G(\omega)|_{\zeta=0} = \frac{C(\omega)}{A(\omega)} \tag{13}$$

When $\zeta = \infty$, the frequency transfer function is:

$$G(\omega)|_{\zeta=\infty} = \frac{D(\omega)}{B(\omega)} \tag{14}$$

In other cases, the frequency transfer function can be expressed as follows:

$$G(\omega)\Big|\zeta = \left(\frac{D(\omega)}{B(\omega)}\right)\left(\frac{C(\omega)/D(\omega) + \zeta}{A(\omega)/B(\omega) + \zeta}\right) = \frac{D(\omega)}{B(\omega)} \tag{15}$$

Clearly: $\frac{C(\omega)}{D(\omega)} = \frac{A(\omega)}{B(\omega)}$ or $\frac{C(\omega)}{A(\omega)} = \frac{D(\omega)}{B(\omega)}$; where ζ is any real number.

Then, the frequency transfer function is shown as follows:

$$G(\omega)|_{\zeta=0} = G(\omega)|_{\zeta=\infty} \tag{16}$$

When $\zeta = 0$ or $\zeta = \infty$, the intersection of the frequency transfer function and ζ is irrelevant, and the intersection is the maximum value of the frequency response curve, which determines that the value of ζ is the optimal damping value. When we designed the SMA-SPDS parameters, the optimum tuning value of the damping device was obtained by using the fixed point heights.

For the optimal design of a multiple degree-of-freedom system damping device, the multiple degree-of-freedom damping system can be decoupled into several single-degree-of-freedom damping systems by using the previous modal analysis, and the corresponding frequency transfer function was obtained, as shown in Equation (14). Using Equations (14)–(20), the optimal design conditions for the i-th single degree-of-freedom

damping device of the modal model was used to determine the main parameters in the SMA-SPDS as follows:

$$\text{Optimal tuning}: \frac{\omega_i}{\Omega_i} = \frac{1}{1+\mu_i} \tag{17}$$

$$\text{Optimal damping ratio}/\%\ \zeta_i = \sqrt{\frac{3\mu_i}{8(1+\mu_i)}} \tag{18}$$

$$\text{Maximum amplitude factor}: \left(\frac{X}{X_{st}}\right)_{max} = \sqrt{1+\frac{2}{\mu_i}} \tag{19}$$

$$\text{Damping device frequency}: \omega_i = \sqrt{\frac{g}{l}+\frac{k_{eq}}{m}\left(\frac{m}{l}\right)^2} \tag{20}$$

where ω_i represents the i-th natural frequency of the mode damper device, Ω_i is the i-th natural frequency of the modal structure, ζ_i is the damping ratio of the i-th mode, k_{eq} is the equivalent secant stiffness of the SMA wire, l is the effective length of the pendulum, μ_i is the mass ratio of the i-th mode, X is the amplitude of mode i, and X_{st} is the maximum displacement that the device can achieve.

After the SMA-SPDS installation location was determined, the target damping ratio of the SMA-SPDSs under each modal control was designed as $\zeta_1 = 0.11$, $\zeta_2 = 0.078$, and $\zeta_3 = 0.05$. According to Equation (19), the mass ratio of SMA-SPDS for each modal setting was determined as $\mu_1 = 0.03$, $\mu_2 = 0.02$, and $\mu_3 = 0.007$. Thus, the parameters of each SMA-SPDS were determined, as shown in Table 8.

Table 8. The recommended design value of the SMA-SPDS parameters for the prototype structure of the Small Wild Goose Pagoda.

	Quality (kg)	Swing Length (m)	SMA Diameter (mm)	Number of SMA
Level one	832	1.534	1.0	6
Level two	634	1.241		4
Level three	459	0.953		4

5.3. Damping Effect

To compare the optimal control effects of the SMA-SPDSs, the top floor of the structure was taken as the research object, and the optimal control effects under different vibration modes were analyzed. Figures 17–22 show the time records of the displacement and acceleration on the top floor of the Small Wild Goose Pagoda with different order modes controlled by different seismic records under the action of an 8-degree earthquake.

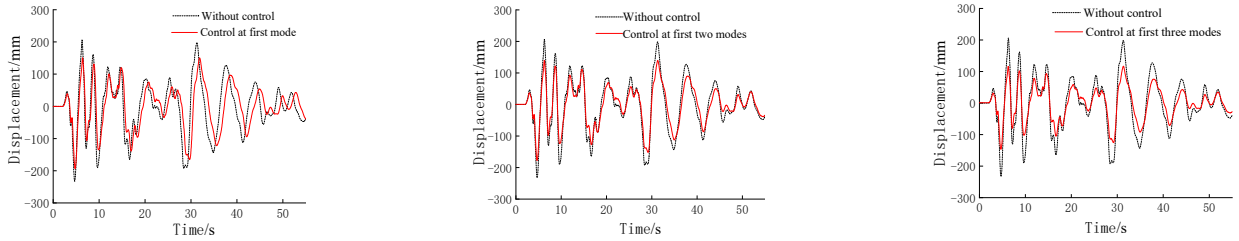

(**a**) (**b**) (**c**)

Figure 17. Time history of displacement by optimized control at different modes under the El-Centro seismic record. (**a**) First mode. (**b**) First two modes. (**c**) First three modes.

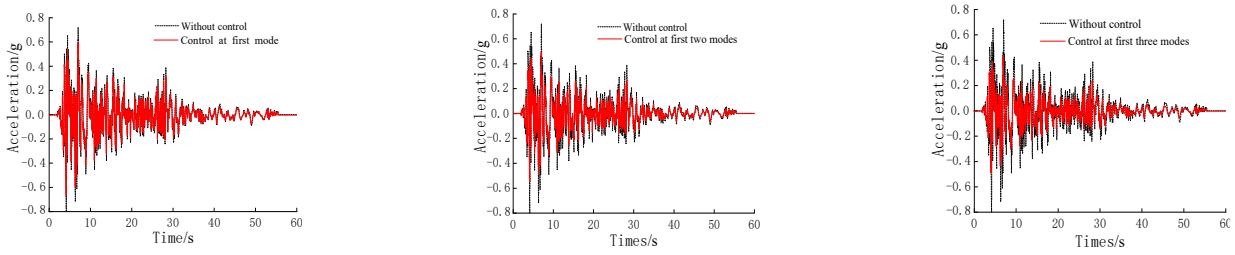

(**a**) (**b**) (**c**)

Figure 18. Time history of acceleration by optimized control at different modes under the El-Centro seismic record. (**a**) First mode. (**b**) First two modes. (**c**) First three modes.

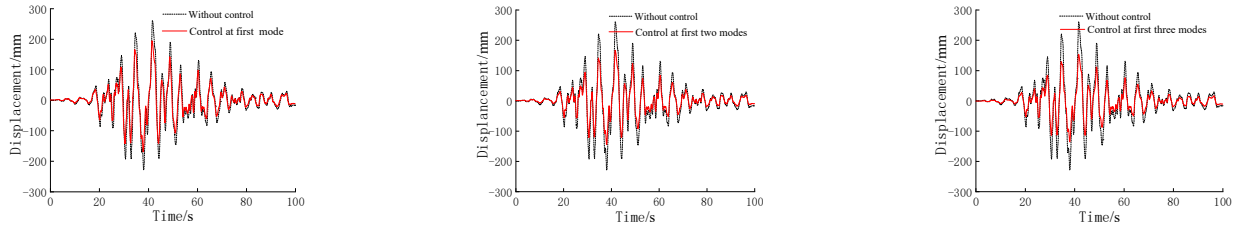

(**a**) (**b**) (**c**)

Figure 19. Time history of displacement by optimized control at different modes under the Jiangyou seismic record. (**a**) First mode. (**b**) First two modes. (**c**) First three modes.

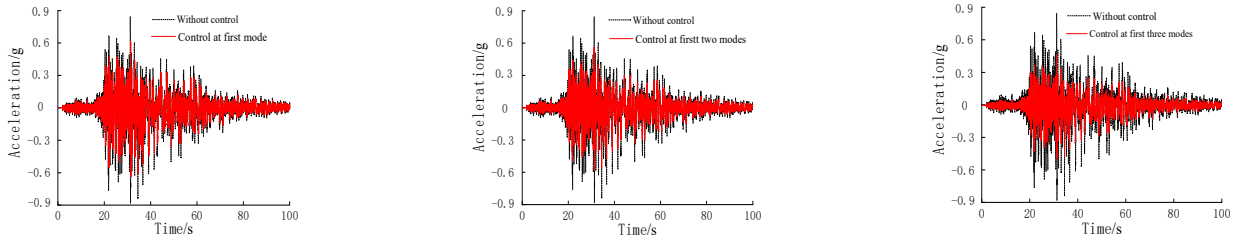

(**a**) (**b**) (**c**)

Figure 20. Time history of acceleration by optimized control at different modes under the Jiangyou seismic record. (**a**) First mode. (**b**) First two modes. (**c**) First three modes.

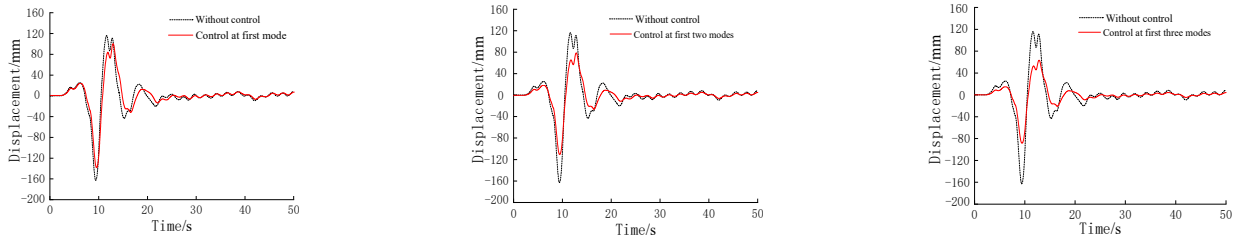

(**a**) (**b**) (**c**)

Figure 21. Time history of displacement by optimized control at different modes under the artificial wave. (**a**) First mode. (**b**) First two modes. (**c**) First three modes.

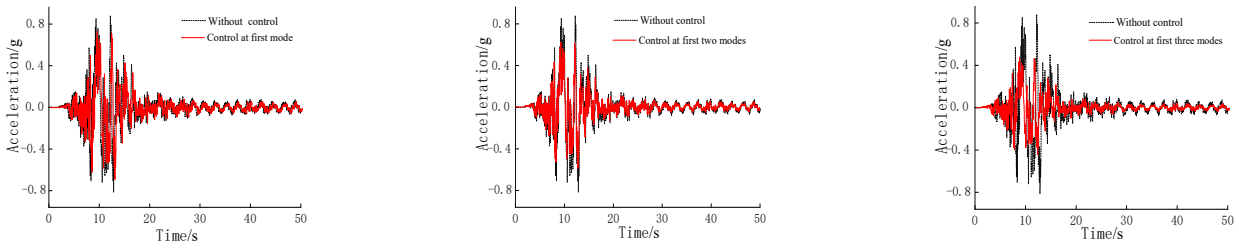

(**a**) (**b**) (**c**)

Figure 22. Time history of displacement by optimized control at different modes under the artificial wave. (**a**) First mode. (**b**) First two modes. (**c**) First three modes.

Tables 9 and 10 show the maximum displacement and acceleration of the top level of the Small Wild Goose Pagoda obtained by optimally controlling the first mode, the first two modes, and the first three modes of the structure, with and without the SMA-SPDSs, under the 8-degree large earthquake (see Tables 9 and 10). A control effect coefficient α was introduced to reflect the control effect of the SMA-SPDSs on the seismic response of the Small Wild Goose Pagoda structure.

$$\alpha = \frac{|X|N - |X|Y}{|X|N}$$

where $|X|N$ is the seismic response of the Small Wild Goose Pagoda structure without the SMA-SPDSs, and $|X|Y$ is the seismic response of the Pagoda structure with the optimized SMA-SPDSs.

Table 9. Comparison of the optimal control displacement with SMA-SPDS.

Seismic Wave	Number of Modes under Control	Maximum Displacement of Structure (mm)		
		Without Control	Optimized Control	α
El-Centro	First one	232.96	191.06	17.9%
	First two		163.25	29.9%
	First three		140.28	39.8%
Jiangyou	First one	266.34	211.63	23.5%
	First two		183.34	33.7%
	First three		152.89	44.7%
Artificial wave	First one	163.45	133.52	18.3%
	First two		108.71	33.5%
	First three		86.84	46.9%

Table 10. Comparison of the optimal control acceleration with SMA-SPDS.

Seismic Wave	Number of Modes under Control	Maximum Displacement of Structure (mm)		
		Without Control	Optimized Control	α
El-Centro	First one	0.81	0.68	16.0%
	First two		0.55	32.1%
	First three		0.50	38.2%
Jiangyou	First one	0.87	0.63	27.5%
	First two		0.60	31.0%
	First three		0.47	46.0%
Artificial wave	First one	0.83	0.77	7.2%
	First two		0.58	30.1%
	First three		0.45	45.8%

The analysis of Figures 17–22 shows that by controlling different order modes, the displacement and acceleration of the original structure of the Small Goose Pagoda were

controlled. The control of the top floor increased significantly with the number of modes that we controlled on the Small Wild Goose Pagoda. Table 10 shows that when the first two modes of the original structure of the Pagoda were controlled, the displacement response of the structure was 32.4% lower, and the acceleration was 31.1% lower on average under the action of the 8-degree shock. When controlling the first three modes, the displacement and acceleration responses of the Pagoda decreased by averages of 43.8% and 43.3%, respectively. We emphasize that more SMA-SPDSs are required to control more modes. The control effect on the Small Wild Goose Pagoda was significantly improved by using more SMA-SPDSs.

Considering the complexity, cost, and operability of actual engineering projects, these results suggest controlling the first three vibration modes of the prototype structure of the Small Wild Goose Pagoda.

6. Conclusions

In this study, the damping protection of the Small Wild Goose Pagoda in Xi'an was taken as the research object. Field investigations, experimental research, theoretical analysis, and numerical simulations were conducted to study the damping control of the Pagoda structure based on an SMA-SPDS. The main conclusions are as follows:

(1) The simulation model of the Small Wild Goose Pagoda with the SMA-SPDS was established by using Simulink. The seismic response of the Small Wild Goose Pagoda model under an 8-degree earthquake was studied and compared with the test results obtained using a shaking table. The comparison showed that the simulation analysis results and experiments were in good agreement. This finding indicated that the proposed method using a simulation model can be employed to study the Small Wild Goose Pagoda, with or without an SMA-SPDS on site.

(2) The Simulink model of the Small Wild Goose Pagoda was employed to calculate the seismic responses of the original structure under 8-degree small, medium, and large earthquakes. The results showed that when the original structure of the Small Wild Goose Pagoda was equipped with a damping system, the frequency of each step increased, which indicated that the SMA-SPDS improved the integrity of the original structure and enhanced its seismic performance. The SMA-SPDS had a significant effect on reducing the seismic response of the Small Wild Goose Pagoda. With increasing seismic intensity, the damping effect significantly reduced the inter-floor displacement angle. The displacement angle between the floors under a large earthquake can be reduced by more than 50%.

(3) For the original structure of the Small Wild Goose Pagoda, the parameters and arrangement of the SMA-SPDS were optimized. The seismic responses of the original Pagoda structure with the SMA-SPDS were compared before and after optimization. Figures 13–18 show that by controlling different numbers of modes, the displacement and acceleration of the original structure of the Pagoda can be controlled. In addition, with the increment of the controlling mode number, the control effect of the top floor on the Pagoda significantly increased. When the first three modes were under control, the displacement and acceleration responses of the Small Wild Goose Pagoda were significantly lower—by 43.8% and 43.3%, respectively.

(4) The protection provided by the SMA-SPDSs on the Small Wild Goose Pagoda strictly follows the principle of minimum intervention for the seismic protection of an ancient tower. The SMA-SPDSs can effectively reduce the structural response of the Pagoda under earthquakes. The proposed protection method has a certain value to both research and engineering communities for applications to similar ancient tower structures.

Author Contributions: Conceptualization, T.Y. and S.L.; methodology, T.Y.; software, T.Y.; validation, Y.L., S.X. and S.L.; formal analysis, S.L.; investigation, S.X.; data curation, B.L.; writing—original draft preparation, T.Y.; writing—review and editing, S.L.; visualization, S.X.; supervision, B.L. All authors have read and agreed to the published version of the manuscript.

Funding: This research was funded by the Shaanxi Provincial Key Research and Development Program (No. 2022SF-375, the funder: B.L.) and the Innovation Capability Support Program of Shaanxi Province (No. 2020PT-038, the funder: B.-B.L.).

Informed Consent Statement: Informed consent was obtained from all subjects involved in the study.

Data Availability Statement: The authors confirm that the data supporting the findings of this study are available within the article.

Conflicts of Interest: The authors declare no conflict of interest.

References

1. Zhang, Y.H. *Ancient Pagoda Record*; Huazhong University of Science and Technology Press: Wuhan, China, 2011.
2. Lu, J.L.; Li, X.L.; Tian, P.G. Study on dynamic characteristics and structural damage identification of Xiaoyan Pagoda. *Build. Struct.* **2019**, *49*, 38–43.
3. Abruzzese, D.; Miccoli, L.; Yuan, J.L. Mechanical behavior of leaning masonry Huzhu Pagoda. *J. Cult. Herit.* **2009**, *10*, 480–486. [CrossRef]
4. Li, S.W.; Wei, J.W.; Li, T.Y.; Li, Q.M.; Bell, A.J. Assessment of Repairs and Strengthening of a Historic Masonry Pagoda Using a Vibration-Based-Method. *J. Struct. Eng.* **2009**, *135*, 67–77. [CrossRef]
5. Shakya, M.; Varum, H.; Vicente, R.; Costa, A.; Bell, A.J. Seismic vulnerability assessment methodology for slender masonry structures. *Int. J. Archit. Herit.* **2018**, *12*, 1297–1326. [CrossRef]
6. Ferraioli, M.; Lavino, A.; Abruzzese, D.; Avossa, A.M. Seismic Assessment, Repair and Strengthening of a Medieval Masonry Tower in Southern Italy. *Int. J. Civ. Eng.* **2020**, *18*, 967–994. [CrossRef]
7. Zhou, Y.; Zhang, F.; Wang, S.L. Structural Protection of Ancient Masonry Pagodas Based on Modified Epoxy Resin Infiltration. journal of new materials for electrochemical systems. *J. New Mater. Electrochem. Syst.* **2020**, *23*, 13–19. [CrossRef]
8. Hadzima-Nyarko, M.; Ademovic, N.; Pavic, G.; Sipos, T.K. Strengthening techniques for masonry structures of cultural heritage according to recent Croatian provisions. *Earthq. Struct.* **2018**, *15*, 479–485.
9. Zhao, X.; Shang, T.W.; Xie, Q.F.; Qian, C.Y. Performance analysis of Small Wild Goose Pagoda seismic reinforcement based on engineered cementitious composite. *China Earthq. Eng. J.* **2017**, *39*, 829–835.
10. Habieb, A.B.; Valente, M.; Milani, G. Effectiveness of different base isolation systems for seismic protection: Numerical insights into an existing masonry bell tower. *Soil Dyn. Earthq. Eng.* **2019**, *125*, 105752. [CrossRef]
11. Elias, S.; Matsagar, V. Research developments in vibration control of structures using passive tuned mass dampers. *Annu. Rev. Control* **2017**, *44*, 129–156. [CrossRef]
12. Cimellaro, G.P.; Lavan, O.; Reinhorn, A.M. Design of passive systems for control of inelastic structures. *Earthq. Eng. Struct. Dyn.* **2009**, *38*, 783–804. [CrossRef]
13. Zhu, R.Z.; Guo, T.; Mwangilwa, F. Development and test of a self-centering fluidic viscous damper. *Adv. Struct. Eng.* **2020**, *23*, 2835–2849. [CrossRef]
14. Shabani, A.; Alinejad, A.; Teymouri, M.; Costa, A.N.; Shabani, M.; Kioumarsi, M. Seismic Vulnerability Assessment and Strengthening of Heritage Timber Buildings: A Review. *Buildings* **2021**, *11*, 661. [CrossRef]
15. Fang, C.; Wang, W.; Zhang, A.; Sause, R.; Ricles, J.; Chen, Y.Y. Behavior and Design of Self-Centering Energy Dissipative Devices Equipped with Superelastic SMA Ring Springs. *J. Struct. Eng.* **2019**, *145*, 04019109. [CrossRef]
16. Qiu, C.X.; Fang, C.; Liang, D.; Du, X.L.; Yam, M.C.H. Behavior and application of self-centering dampers equipped with buckling-restrained SMA bars. *Smart Mater. Struct.* **2020**, *29*, 035009. [CrossRef]
17. Wang, W.; Fang, C.; Zhang, A.; Liu, X.S. Manufacturing and performance of a novel self-centering damper with shape memory alloy ring springs for seismic resilience. *Struct. Control Health Monit.* **2019**, *26*, e2337. [CrossRef]
18. Dieng, L.; Helbert, G.; Chirani, S.A.; Lecompte, T.; Pilvin, P. Use of Shape Memory Alloys damper device to mitigate vibration amplitudes of bridge cables. *Eng. Struct.* **2013**, *56*, 1547–1556. [CrossRef]
19. Behrouz, A.; Neda, S.; Behnam, S. Application of Intelligent Passive Devices Based on Shape Memory Alloys in Seismic Control of Structures. *Structures* **2016**, *5*, 161–169.
20. Kari, A.; Ghassemieh, M.; Abolmaali, S.A. A new dual bracing system for improving the seismic behavior of steel structures. *Smart Mater. Struct.* **2011**, *20*, 125020. [CrossRef]
21. Zhang, M.Z. Study on similitude laws for shaking table tests. *Earthq. Eng. Eng. Dyn.* **1997**, *17*, 52–58.
22. *GB50003-2011*; Code for Masonry Structure Design: GB50003-2011. China Building Industry Press: Beijing, China, 2011.

23. Yang, F.; Sedaghati, R.; Esmailzadeh, E. Vibration suppression of structures using tuned mass damper technology: A state-of-the-art review. *J. Vib. Control* **2022**, *28*, 812–836. [CrossRef]
24. Capanna, I.; Cirella, R.; Aloisio, A.; Di Fabio, F.; Fragiacomo, M. Operational Modal Analysis and Non-Linear Dynamic Simulations of a Prototype Low-Rise Masonry Building. *Buildings* **2021**, *11*, 471. [CrossRef]